HHS Public Access

Author manuscript

*Neurobiol Dis*. Author manuscript; available in PMC 2021 March 15.

Published in final edited form as:

*Neurobiol Dis*. 2020 August ; 142: 104959. doi:10.1016/j.nbd.2020.104959.

# Disrupted inhibitory plasticity and homeostasis in Fragile X syndrome

**C.A. Cea-Del Rio**[a,b,c], **A. Nunez-Parra**[d,e], **S.M. Freedman**[a], **J.K. Kushner**[a,f], **A.L. Alexander**[f], **D. Restrepo**[d], **M.M. Huntsman**[a,g,*]

[a]Department of Pharmaceutical Sciences, Skaggs School of Pharmacy and Pharmaceutical Sciences, University of Colorado, Anschutz Medical Campus, Aurora, CO, United States of America

[b]CIBAP, Escuela de Medicina, Facultad de Ciencias Medicas, Universidad de Santiago de Chile, Santiago, Chile

[c]University of Colorado, Anschutz Medical Campus, Aurora, CO, United States of America

[d]Department of Cell and Developmental Biology, School of Medicine, University of Colorado, Anschutz Medical Campus, Aurora, CO, United States of America

[e]Department of Biology, Universidad de Chile, Santiago, Chile

[f]Department of Neurosurgery, School of Medicine, Anschutz Medical Campus, Aurora, CO, United States of America

[g]Department of Pediatrics, School of Medicine, University of Colorado, Anschutz Medical Campus, Aurora, CO, United States of America

## Abstract

Fragile X Syndrome (FXS) is a neurodevelopmental disorder instigated by the absence of a key translation regulating protein, Fragile X Mental Retardation Protein (FMRP). The loss of FMRP in the CNS leads to abnormal synaptic development, disruption of critical periods of plasticity, and an overall deficiency in proper sensory circuit coding leading to hyperexcitable sensory networks. However, little is known about how this hyperexcitable environment affects inhibitory synaptic plasticity. Here, we show that *in vivo* layer 2/3 of the primary somatosensory cortex of the *Fmr1* KO mouse exhibits basal hyperexcitability and an increase in neuronal firing rate suppression during whisker activation. This aligns with our *in vitro* data that indicate an increase in GABAergic spontaneous activity, a faulty mGluR-mediated inhibitory input and impaired inhibitory plasticity processes. Specifically, we find that mGluR activation sensitivity is overall diminished in the *Fmr1* KO mouse leading to both a decreased spontaneous inhibitory postsynaptic input to principal cells and a disrupted form of inhibitory long-term depression (I-LTD). These data suggest an adaptive mechanism that acts to homeostatically counterbalance the cortical hyperexcitability observed in FXS.



*Corresponding author at: Department of Pharmaceutical Sciences, Skaggs School of Pharmacy and Pharmaceutical Sciences, Department of Pediatrics School of Medicine, University of Colorado, Anschutz Medical Campus, Aurora, CO 80045, United States of America. Molly.Huntsman@CUAnschutz.edu (M.M. Huntsman).

**Keywords**

Inhibitory neurotransmission; Plasticity; Fragile X syndrome; Interneurons; Cortex

## 1. Introduction

FMRP is implicated in the transport of approximately 4–8% of all synaptic mRNAs and regulates the translation of numerous proteins involved in synaptic transmission and receptor systems (Brown et al., 2001). Defects underlying FXS and autism spectrum disorders are widely believed to lie at the level of the synapse (Zoghbi, 2003; Ebert and Greenberg, 2013) affecting both excitatory and inhibitory neurotransmission across multiple brain regions leading to hyperexcitable sensory circuits (Huber et al., 2002; Olmos-Serrano et al., 2010; Paluszkiewicz et al., 2011). Clinically, children with FXS reflect heightened response to somatosensory stimuli, and this manifests itself behaviorally as sensory “defensiveness”, characterized as retreating or pulling away when touched (Miller et al., 1999; Hagerman and Stafstrom, 2009). This hypersensitive phenotype has also been described in the mouse model of FXS (*Fmr1* KO mice) whom have deficits in whisker-tactile learning tasks due to a hyperactive response to sensory activity (Arnett et al., 2014; He et al., 2017). Overall, this altered cortical response may support the hypothesis that a highly active network fails to adequately decipher sensory inputs due to inadequate excitatory/inhibitory (E/I) balance and deficiencies in proper plasticity mechanics within the neocortex.

Synaptically, the best documented consequence of FMRP loss is the lack of translation repression of mGluRs (Bagni and Greenough, 2005). The “mGluR theory” of FXS [reviewed in (Bear et al., 2004)] accounts for the diverse neurological phenotypes associated with uncontrolled mGluR-mediated protein-synthesis-dependent functions. Yet, while mGluR-mediated excitatory synaptic function and plasticity has been previously studied in FXS, little is known about how the mGluR theory plays into inhibitory synaptic mechanisms (El Idrissi et al., 2005; D’Hulst et al., 2006; Gibson et al., 2008; Olmos-Serrano et al., 2010; Martin et al., 2014). Therefore, considering that sensory input computation and interpretation are heavily dependent on inhibitory network function [reviewed in (Maffei, 2017)], it is important to understand how the aberrant glutamatergic and mGluR modulation seen in FXS alters inhibitory circuits of the primary somatosensory cortex (S1).

In this study, we show that *in vivo Fmr1* KO mice have alterations in sensory processing in layer 2/3 (L2/3) of S1 and that neurons within this region are hyperexcitable and are differentially modulated by mGluR activation. This is further emphasized in *in vitro* recordings which demonstrate that mGluR activation has a diminished impact on inhibitory synaptic activity and fails to drive I-LTD in *Fmr1* KO mice. This altered response seems to primarily be due to a decrease in the mGluR sensitivity rather than mGluR-mediated activation *via* endocannabinoid signaling, that could also be accounted for by a ceiling effect of the cortical network activity. We find that the disturbance in mGluR synaptic and neuromodulatory function, has a significant impact on inhibitory plasticity. Overall, we believe that this hyperexcitable phenotype observed in the *Fmr1* KO mouse induces changes in the inhibitory drive of the network in a mGluR-dependent manner, possibly as a

homeostatic counterbalance mechanism that can directly affect the computational processes occurring in L2/3 of S1 thereby disrupting sensory perception capabilities.

## 2. Materials and methods

### 2.1. Mice

All experiments were performed under protocols approved by the Ethics and Animal Care Committee of the University of Colorado|Anschutz Medical Campus (Protocol#00039). Both WT and *Fmr1* KO mice were acquired from Jackson Laboratories (Bar Harbor, ME, USA) and bred onsite. The *Fmr1* KO mice obtained from these crosses were tested *via* genotyping protocols. Male mice utilized in this study possess the same congenic FVB background and only X chromo-some *Fmr1* gene hemizygotes were utilized for the experiments in this research. Neonatal mice were housed with their respective mothers before weaning.

### 2.2. In vivo recordings

Extracellular recordings in anesthetized and awake behaving mice were performed as previously described (Doucette et al., 2011; Gire et al., 2013; Li et al., 2014; Li et al., 2015a). Briefly, four tetrodes consisting of four polyimide-coated nichrome wires (diameter 12.5 μm, Sandvik) were connected to a 16-channel interface board (EIB-16, Neuralynx) and fed through a housing glued to the board. Immediately before implantation the tetrodes were gold-plated to an impedance of 200–350 MΩ. Adult mice (P60–90) were anesthetized with an intraperitoneal injection of ketamine (100 mg/kg) and xylazine (10 mg/kg) and were then implanted with the tetrodes in layer 2/3 at co-ordinates AP:−1.46 mm, ML: 3 mm. On the day of surgery, the electrodes were implanted 200 μm above the final location and every day it was lowered 50 μm until reaching a final depth of DV: 1 mm, respectively. A screw was also implanted in the skull in the opposite hemi-sphere (1 mm right and 2 mm posterior of bregma) to serve as a ground reference. The mice were allowed to recover at least one week before experiments were performed. On the day of the experiment, mice were placed in an 18×12×12 cm anesthesia plexiglass chamber, customized to deliver air puffs through a port while a 1% isoflurane in 2:1 oxygen/nitrogen inhalant was delivered using a SurgiVet model 100 vaporizer. Animal reflex responses were checked throughout to test for anesthetization. Before recording, mice were placed next to the air puff port and positioned to get the maximal contralateral neuronal response. Whiskers were then stimulated with a ~ 3 L/min air puff. The output of the tetrodes was connected to a 16-channel amplifier (A-M Systems 3500) through a 1× gain headstage (Tucker-Davis Technologies). The signal was amplified 1000× and was recorded digitally at 24 kHz with a Data Translation DT3010 A/D card in a PC computer controlled with a custom MATLAB (Mathworks) program. Spike clustering analysis was performed as is explained in detail in (Li et al., 2015b). Briefly, data was filtered digitally between 300 and 3000 Hz. Then, using custom written MATLAB programs, each of the 16 channels were put at a threshold that was three times the standard deviation of the mean. Every spike with an amplitude greater than the threshold was imported into a second program (1 ms record per spike) which performed superparamagnetic clustering and wavelet decomposition of the spikes using 13 different wavelets and three principal components (Quiroga et al., 2004).

To determine the responsiveness of the units to the different events, we aligned all trials to the starting point of the event and calculated the average firing rate (FR, in Hz). FR was calculated for 500 ms before the air puff (baseline) and for 1 s after the air puff (air) was delivered. A paired samples *t*-test was performed to compare before and after the event and the *p*-value was corrected for multiple comparisons using the false discovery rate (Curran-Everett, 2000). To display the results, the FR was calculated in 0.1 s bins and normalized per unit to the mean FR 1 s before the beginning of the event.

For the (*S*)-3, 5-Dihydroxyphenylglycine (DHPG) infusion experiments, a cannula (Plastics One Inc.) was attached to the implant housing and the same surgical protocol was performed. Once the mice recovered from surgery, twenty 9 s trials were recorded in the awake freely moving mouse. Then, 3 μL of DHPG (100 μM) were infused under anesthesia (1% isoflurane) at a rate of 1 μL/min. 30 min after the infusion (when the mouse was fully awake), twenty 9 s trials were recorded. The FR of the twenty trials before and after DHPG infusion was averaged. Student's *t*-test, KeS tests, and Chi-Square test were applied to test for statistical significance.

### 2.3. Slice preparation

Postnatal 19 to 25-day old WT and *Fmr1* KO mice were anesthetized by $CO_2$ inhalation and decapitated. This age range was used, because this is the developmental time point when inhibitory neurotransmission and inhibitory interneurons have reached maturity (Huntsman and Huguenard, 2000; Doischer et al., 2008; Goldberg et al., 2011). Brains were removed and initially placed in a 4 °C oxygenated sucrose slicing solution for 2 min and was composed of (in mM): 234 sucrose, 11 glucose, 26 $NaHCO_3$, 2.5 KCl, 1.25 $NaH_2PO_4$ 10, $MgSO_4$, and 0.5 $CaCl_2$ (equilibrated with 95% $O_2$ and 5% $CO_2$, pH 7.4). Coronal slices were obtained at a 300-μm-thickness using a Vibratome (Leica VT1200S, Leica Biosystems, Buffalo Grove, IL, USA). Then slices were hemisected and incubated in pre-warmed (36 °C), oxygenated artificial cerebrospinal fluid (ACSF; in mM): 126 NaCl, 26 $NaHCO_3$, 10 glucose, 2.5 KCl, 1.25 $NaH_2PO_4$, 2 $MgCl_2$, and 2 $CaCl_2$) for 45–60 min before being transferred to the recording chamber, where they were continuously perfused with oxygenated ACSF at 32–36 °C.

### 2.4. Electrophysiology

Recordings were obtained from pyramidal cells in primary somatosensory cortex L2/3 in WT and *Fmr1* KO mice. Slices were visually identified using differential interference contrast (DIC) on a modified Olympus upright microscope (Scientifica, East Sussex, United Kingdom). Whole-cell recordings were performed with a Multiclamp 700B amplifier (Molecular Devices Corp., Sunnyvale, CA, USA), using recording pipettes (3–5 MΩ) pulled on a PC10 vertical puller (Narishige International, Amityville, NY, USA). Individual spontaneous inhibitory postsynaptic currents (sIPSCs) were isolated by bath applying NMDA and AMPA receptor antagonists (50 μM D-APV and 10 μM DNQX) while holding L2/3 pyramidal cells at −60 mV in voltage-clamp mode. Spontaneous excitatory postsynaptic currents (sEPSCs) were isolated by blocking $GABA_A$R-mediated currents (5 μM gabazine) while holding L2/3 pyramidal cells at −60 mV in voltage-clamp mode. Recording pipettes were filled with an intracellular solution containing (in mM): 90

$CsCH_3SO_4$, 1 $MgCl_2$, 50 CsCl, 2 MgATP, 0.2 $Cs_4$-BAPTA, 10 HEPES, 0.3 Tris GTP, and 5 QX314 for sIPSCs, I-LTD, and depolarization-induced suppression of the inhibition (DSI) recordings. For sEPSC recordings, pipettes were filled with an intracellular solution containing (in mM): 135 potassium gluconate, 20 KCl, 10 Hepes, 0.1 EGTA, 2 MgATP, and 0.3 $Na_2GTP$. For all recordings, series resistance (Rs) was monitored throughout each voltage-clamp recording with 50 ms, −10 mV steps every 4 s for drug application and DSI experiments, and every 15 s for the I-LTD experiments. Recordings where Rs changed more than 20% were discarded. Recordings were low-pass filtered at 4 kHz (Bessel filter) and digitized at 10 kHz (Digidata 1440) using pClamp 10.3 software (Molecular Devices Corp., Sunnyvale, CA, USA).

### 2.5. Spontaneous postsynaptic experiments

For sIPSC/sEPSC recordings, we recorded 5 min of basal activity followed by 5 min of drug bath application (DHPG or carbachol (10 μM)). Five different DHPG concentrations were tested (1, 2, 5, 10, 100 μM) in this study, and only one concentration per pyramidal cell was recorded per slice. For analysis, postsynaptic events were visually identified using pre-written custom code routines in Axograph-X. For each recording, three 30 s time frames (at 30 s, 2.5 min, and 4.5 min) were analyzed from the 5 min. For drug recording conditions, time frames were taken after 2 min of bath application (which is the turnout point for the whole volume bath). These events were analyzed by comparing amplitude and frequency within and between WT and *Fmr1* KO mice, and paired and unpaired *t*-tests were applied respectively for statistical comparison. Differences in the magnitude of the DHPG responses between WT and *Fmr1* KO mice were further analyzed by one-way anova test. A wash-out of the respective drug for 10 min was performed before the next slice was added to the recording chamber.

### 2.6. I-LTD experiments

For electrically induced I-LTD experiments, evoked IPSCs (eIPSCs) were elicited by 1-ms-long extracellular stimuli using a concentric microelectrode (FHC) placed in layer 4 of the somatosensory cortex every 15 s. Stimulation amplitude was calculated by the 50% of the maximum amplitude response of the IeO curve (for consistency we maintained response amplitude and not stimulation amplitude for our recordings). After 5 min of stable baseline, electrical I-LTD was induced by high-frequency stimulation (HFS), which consisted of 2 trains (20s apart), each containing 100 pulses at 100 Hz. For chemically induced I-LTD, 5 min of baseline was recorded followed by 10 min of 10 μM of DHPG or 10 μM of muscarine and then washed-out for the rest of the experiment time. For drug bath application experiments, AM251 (4 μM), a combination of MPEP (4 μM) (2-Methy-6-(phenylethynyl)pyridinehy-drochloride) and LY367385 (100 μM) ((*S*)-(+)-α-Amino-4-carboxy-2-methylbenzeneaceticacid), and H89 (10 μM) (N-[2-[[3-(4-Bromophenyl-2-propenyl]amino]ethyl]-5-iso-qunolinesulfonamidedihydrochloride) were pre-incubated for 10 min before the I-LTD experiment and bath applied throughout the whole experiment. For all I-LTD experiments, recordings were 40 min long and performed in the continuous presence of NMDA and AMPA receptor antagonists (50 μM D-APV and 10 μM DNQX). The magnitude of I-LTD was estimated by comparing the average amplitude of responses for each minute from 30 to 40 min of recording to baseline-averaged responses one minute

before induction. We also compared averaged amplitude responses from 4 to 7 min of recordings after electrical or chemically-induced protocols to baseline-averaged responses one minute before induction to estimate short term depression of the inhibition (I-STD). For statistical analyses purposes, we performed a paired *t*-test to determine the expression of I-LTD and we reported *p*-values for 5 min and 35 min after induction. Additionally, a one-way anova test was used for statistical comparisons to determine differences in the I-LTD response between genotypes.

### 2.7. DSI experiments

For DSI experiments, sIPSCs were recorded in the presence of carbachol (20 μM) for 4 min before DSI was evoked. DSI was evoked by a 1 s voltage step from −60 to 0 mV. DSI magnitude was measured as the percentage of change between the mean of the ten consecutive IPSCs preceding the depolarization and the mean of three IPSCs immediately following depolarization (acquired 3–12 s after the pulse). In a subset of experiments AM251 (4 μM) was added with carbachol for related experiments. To determine whether DSI was evoked a paired t-test was performed for statistical comparisons.

For Win55-212-2 (Win55) experiments, evoked IPSCs (eIPSCs) were elicited by 1-ms-long extracellular stimuli using a concentric microelectrode (FHC) placed in layer 4 of the somatosensory cortex every 15 s, as described above as electrically induced I-LTD. After two minutes of baseline recording, Win55 (5 μM) was bath-applied for 5 min and then washed-out for 15 min while recording. Statistical comparisons were made between minute 1 (baseline) and minute 10 (Win55 effective steady state) and between genotypes using unpaired and paired *t*-tests, respectively.

### 2.8. Statistical analysis

Data were acquired with pClamp10 and Analyzed with Axograph-X and MatLab. All data was tested for normality using the Shapiro-Wilk test. Accepted scale of *p*-values for the entire text were used (* = $P \leq .05$, ** = $P \leq .01$, *** = $P \leq .001$, **** = $P \leq .0001$). All error bars represent standard deviation unless otherwise noted.

## 3. Results

### 3.1. Cortical response to sensory stimulation recorded in vivo

Cortical hyperexcitability is prevalent in FXS and in the *Fmr1 KO* mouse model [reviewed in (Contractor et al., 2015)]. Therefore, we initially wanted to quantify this hyperexcitability by *in vivo* tetrode recordings of cellular responses at baseline and to whisker stimulation in L2/3 in anesthetized and awake behaving WT and *Fmr1* KO mice (P60–90). The setup for tetrode recording neuronal activity in L2/3 in the anesthetized mouse is shown (Fig. 1A). Offline spike analyses of tetrode recordings revealed that the baseline rate of the recorded units (before stimulation of the whisker) was higher in *Fmr1* KO mice, (Fig. 1B, t-test $p < .02$, KeS test $p < .005$; $n = 29$ units from 3 WT and $n = 24$ units from 3 *Fmr1* KO) which is consistent with network hyperexcitability in these mice. Next, we stimulated the contralateral whiskers with an air puff in anesthetized mice and calculated the delta firing rate (FR) before and after the stimulus. We found that a subset of cells responded

differentially (determined with a t-test corrected for multiple comparison of 1 s before the puff and 500 ms after, $p < .05$) with either increases or decreases in firing rate (FR) in both groups (Fig. 1C and D). Importantly, the units in the *Fmr1* KO mice responded differently than those in the WT mice, with more units exhibiting a decrease in FR after the whiskers were activated (Chi-square test, units decreasing FR: 3 out of 29 in the WT mice *vs* 8 out of 24 in the *Fmr1* KO, $p = .04$; units increasing FR: 4 out of 29 *vs* 2 out of 24 in the WT and *Fmr1* KO, respectively, $p = .5$). The delta change of FR of the units that responded to the stimulus, however, is not significantly different between WT and the *Fmr1* KO. These data suggest that there is a potential alteration in the excitatory/inhibitory balance. Specifically, increased basal FR could indicate a tonic (or static) hyperexcitable environment, and an increase in the number of units that decrease their FR after air puff might indicate that inhibition may also be hyperexcitable in *Fmr1* KO mice.

mGluR activation has been widely studied in FXS models and has been shown to be one of the primary pathways affecting neuronal excitability in FXS (Bear et al., 2004). Therefore, we decided to study the effect of the activation of this receptor *in vivo*. Since the activation of mGluRs varies depending on brain state, specifically modulating neuronal synchronization and excitability, (Kuhn et al., 2008; Song et al., 2018), we decided to infuse the group 1 mGluR agonist, DHPG, in L2/3 of the somatosensory cortex in awake and freely moving mice. We re-designed our implantable recording device by attaching a cannula that allowed us to record electrical activity before and after local DHPG infusion (Fig. 1E). Only units that could be identified in both conditions were included in our analysis. In agreement with our anesthetized mouse data, awake *Fmr1* KO mice exhibited a higher firing rate frequency compared to WT in basal conditions (Fig. 1F, left panel, K–S test $p = .008$; $n = 16$ units and $n = 25$ units from 3 WT and 3 *Fmr1* KO, respectively), suggesting again that *Fmr1* KO neurons are hyperexcited in different brain states. Next, we calculated the delta FR of each of the units before and after 30 min of DHPG (100 μM) infusion (FR after DHPG infusion minus FR before DHPG infusion). We found that some units increased their FR after the drug was applied while others decreased FRs (Fig. 1F, right; 8 units decreased and 8 units increased their FR in the WT while 6 units decreased and 19 increased their FR in the *Fmr1* KO). Interestingly, we found that DHPG infusion did not cause a statistically significant difference in neuronal activity for WT or *Fmr1* KO mice when compared to the control recordings without the drug, but *Fmr1* KO mice did show a tendency toward an overall diminished sensitivity to mGluR activation (Fig. 1F, WT: 97 ± 29.3 Hz and − 13.8 ± 5.1 Hz, KO: 54.6 ± 12.9 Hz and − 18 ± 10.5 Hz, *t*-test $p = .7$ and $p = .1$ WT *vs Fmr1* KO for units decreasing and increasing their FR, respectively). Taken together, our data indicates *in vivo Fmr1* KO S1 L2/3 neurons are hyperexcited, respond differently to sensory stimuli, and possess mGluR sensitivity that resembles that of the WT mouse.

## 4. Decreased neuromodulatory role of mGluRs on inhibitory activity in the somatosensory cortex

In order to determine if E/I balance is also perturbed *in vitro*, we first recorded basal sIPSCs and sEPSCs in L2/3 of the somatosensory cortex in slice. Compared to our previous study, where recordings were made at room temperature, (Paluszkiewicz et al., 2011), we found

that baseline sIPSC frequency was increased in *Fmr1* KOs (KO: 7.12 ± 0.46 Hz, $n = 38$) compared to WT mice (WT: 5.48 ± 0.46 Hz, $n = 32$, $p = .014$), suggesting an augmented basal inhibitory activity in L2/3 of *Fmr1* KO mice (Fig. 2A and B, upper panels and Fig. 2J). Previous reporting by us and others suggests that DHPG increases the frequency of sIPSCs in P19–30 WT mice cortical layer 2/3 pyramidal cells and that DHPG-induced increase in frequency is attenuated in *Fmr1* KOs when higher concentrations of DHPG are applied (100 μM) (Fanselow et al., 2008; Paluszkiewicz et al., 2011). Based on these results, we wanted to assess if mGluR activation is altered in response to physiological levels of glutamatergic activity in FXS. To do this, we examined the effect of DHPG on sIPSCs recorded from pyramidal cells in L2/3 of somatosensory cortex of WT and *Fmr1* KO mice in a range of concentrations from 1 to 100 μM (1, 2, 5, 10, and 100 μM; Fig. 2). When DHPG was bath applied on WT L2/3 pyramidal cells, changes in sIPSCs were noticed as low as 10 μM. Notably, WT sIPSC frequency (from 6.30 ± 0.90 Hz to 11.64 ± 1.20 Hz, $n = 12$, $p = 4.5e\text{-}5$; Fig. 2A, G and K) and amplitude (from 14.75 ± 1.16pA to 21.90 ± 2.47pA, n = 12, $p = .005$; Fig. 2A, G and L) were significantly increased. However, when DHPG (10 μM) was bath applied on L2/3 pyramidal cells from *Fmr1* KO mice, there were significantly smaller changes for sIPSC frequency (from 7.55 ± 0.55 Hz to 10.16 ± 0.91 Hz, $p = .025$, $n = 11$; Fig. 2B, G and K) and no changes were observed in amplitude (from 14.08 ± 1.80pA to 22.04 ± 4.79pA, $p = .1$; n = 11; Fig. 2B, G and L).

When responses were recorded as a function of DHPG concentration for frequency and amplitude as shown in the normalized DHPG to basal sIPSC activity dose-response plots (Fig. 2K and L), differences were found at 10 μM and 100 μM of DHPG between *Fmr1* KO and WT sIPSC frequency, but differences in amplitude were only found at 100 μM. Indeed, when the 10 μM DHPG response was normalized to the baseline frequency activity, the increment of sIPSC frequency was significantly lower in *Fmr1* KO than WT counterparts (sIPSC frequency: 1.25 ± 0.19 Hz, n = 11 *vs* 2.17 ± 0.27 Hz, n = 12; unpaired *t*-test, $p = .039$;. Fig. 2K). Moreover, a one-way anova test indicated that the frequency response to DHPG at 10 μM concentration was different between genotypes ($F = 6,9$: $p = .0007$).

When recording sEPSCs of L2/3 pyramidal cells from WT and *Fmr1* KO mice we found a significant difference in basal sEPSC frequency (WT: 9.84 ± 1.94 Hz, $n = 5$ and *Fmr1* KO:15.19 ± 1.48 Hz, n = 5, t-test $p = .035$, Fig. 2H) indicating elevated basal excitability. We then tested if DHPG affected sEPSCs and found that with 10 μM of DHPG, WT sEPSC frequency significantly increased (9.84 ± 1.94 Hz to 17.50 ± 1.80 Hz, n = 5, $p = .012$). However, neither sEPSC amplitude or frequency were significantly changed in the *Fmr1* KO mice (10.45 ± 0.48pA to 10.25 ± 0.54pA, n = 5, $p = .80$; and from 15.19 ± 1.48 Hz to 15.18 ± 2.01 Hz, n = 5, $p = .99$, respectively; Fig. 2C, D and H), suggesting that mGluR responsiveness is overall affected in the network. In order to understand whether this response is specific for mGluRs or if other neuromodulators are also failing to modulate the inhibitory activity, we bath applied carbachol (10 μM), an agonist of cholinergic receptors. We found that carbachol induced increases of sIPSC frequency (WT: from 4.53 ± 0.54 Hz to 7.73 ± 0.18 Hz, $n = 7$, $p = .0004$; KO: from 4.18 ± 0.53 Hz to 7.66 ± 0.23 Hz, $n = 10$, $p = .0001$) and amplitude (WT: from 16.67 ± 0.79pA to 52.45 ± 10.28pA, n = 7, $p = .014$; KO: from 16.89 ± 0.92pA to 59.60 ± 10.34pA, n = 10, $p = .002$) in both WT and *Fmr1* KO pyramidal cell recordings (Fig. 2E, F and I). These results suggest that cholinergic

neuromodulation on inhibitory activity of the somatosensory cortex is functional and that mGluR-mediated responses are not the result of the altered inhibitory synaptic properties of the network. Altogether, these data indicate there is a basal increase in sIPSCs frequencies and that there is a loss of inhibitory drive mediated by mGluR activation in FXS.

## 5. Heterosynaptic I-LTD is impaired in *Fmr1* KO mice

Several studies have reported the critical roles of mGluR-mediated plasticity in FXS (Nosyreva and Huber, 2006; Bianchi et al., 2009; Zhang et al., 2009; Auerbach and Bear, 2010; Connor et al., 2011; Chevere-Torres et al., 2012; Yau et al., 2016), however there is no information on how plasticity at inhibitory synapses is affected in FXS. A well-known and studied form of heterosynaptic I-LTD is an eCB-mediated I-LTD that is triggered by postsynaptic activation of group I metabotropic glutamate receptors (mGluR-I) in the hippocampus (Chevaleyre and Castillo, 2003). In this case, the mGluR activation leads to the production of diacylglyercol (DAG) by phospholipase C (PLC). In turn, diacylglycerol lipase (DGL) converts DAG to the major eCB, 2-AG, which is released from the postsynaptic cell and travels back across the synapse to activate type 1 cannabinoid receptors (CB1Rs) on the GABAergic terminal. CB1R activation subsequently reduces protein kinase A activity, which combined with an enhancement of Calcineurin (CaN) activity may lower the phosphorylation status of an unidentified substrate in the release machinery to persistently depress GABA release (Castillo et al., 2011).

Considering from our previous data that the inhibitory-mediated mGluR responsiveness was decreased, we wanted to understand whether this heterosynaptic I-LTD may be altered in FXS. To do this, we first induced I-LTD through a protocol of high frequency electrical stimulation (HFS) in layer 4 (L4) of S1 and recorded evoked IPSCs (eIPSCs) from pyramidal cells in L2/3. I-LTD was measured by analyzing the percentage of change of the integral under the curve of the eIPSC before and after the stimulation protocol. We found that L2/3 pyramidal cells responded with a long-lasting depression (60.14 ± 10.42% of the baseline, $n = 8$, $p = .032$; Fig. 3A) indicating our electrical induction of I-LTD worked. We then tested whether the activation of CB1R was necessary for I-LTD to be maintained, like previously reported. To do this, we bath applied AM251 (4 μM), an inverse agonist of cannabinoid receptor type 1 (CB1R), for 10 min before electrically inducing I-LTD. We found that AM251 blocked the electrically mediated I-LTD (96.08 ± 21.01% of the baseline, $n = 4$, $p = .92$; Fig. 3B) suggesting that the activation of CB1R is necessary to mediate the depression of the inhibitory drive into pyramidal cells.

Next, we wondered if we could recapitulate the I-LTD seen in WT in *Fmr1* KOs. To do this, we electrically induced I-LTD in *Fmr1* KO mice and found that eIPSCs recorded from pyramidal cells of *Fmr1* KO mice did not change in response to HFS stimulation (88.60 ± 8.04% of the baseline, $n = 7$, $p = .29$; Fig. 3C) indicating that I-LTD in *Fmr1* KO mice is faulty. To confirm whether the observed WT I-LTD was a heterosynaptic I-LTD, we tested whether mGluRs were critical to this response using a combination of MPEP (4 μM) and LY367385 (100 μM) to block all group I mGluRs. When the MPEP/LY367385 cocktail was applied, eIPSCs in pyramidal cells of WT mice respond differently than the control group to electrical stimulation (one-way anova test, $F = 21.75$: $p < .0001$) and did not exhibit I-LTD

(83.56 ± 5.90% of the baseline, $n = 5$, $p = .13$; Fig. 3D). These data suggest that group I mGluRs participate in the long-term depression synaptic plasticity process. Moreover, since AM251 (4 μM) blocked electrically mediated I-LTD (Fig. 3B), we postulate that mGluR activation may be coupled to the activation of CB1R to mediate the depression of the inhibitory drive into pyramidal cells. Because the heterosynaptic I-LTD also depends on presynaptic PKA activity, we applied H89 (10 μM), an inhibitor of Protein Kinase A (PKA) and found that I-LTD was blocked (97.05 ± 15.06% of the baseline, $n = 3$, $p = .83$; Fig. 3D). This data suggests that the observed I-LTD is heterosynaptic and is dependent on mGluR, CB1R and PKA activation in an input specific manner.

To determine whether heterosynaptic I-LTD could also be triggered by other metabotropic receptors, we tested if the mAchR agonist, muscarine, could elicit I-LTD, since it shares common intracellular signaling pathways with mGluRs (Younts et al., 2013; Younts and Castillo, 2014). Bath application of muscarine (10 μM) induced a long-term depression of inhibitory activity in L2/3 pyramidal cells (60.79 ± 6.34% of the baseline, n = 5, $p = .0008$; Fig. 3E), thereby supporting the fact that mAchR activation can elicit I-LTD in L2/3 of the somatosensory cortex. However, muscarine application onto L2/3 pyramidal cells of *Fmr1*KO mice failed to induce I-LTD (113.73 ± 13.98% of the baseline, $n = 6$, $p = .51$; Fig. 3E) suggesting that I-LTD failure is not only dependent on mGluR activation, but also on the intracellular pathways that are shared with mAchRs. Therefore, these results suggest that group I mGluRs participate in the long-term depression synaptic plasticity process and that faulty I-LTD in FXS is not apparently due to defects in the molecular machinery involved in this phenomena and could be result of a diminished mGluR responsiveness associated to the hyperactive network.

To further evaluate this hypothesis, we tested whether chemical activation of mGluRs could elicit I-LTD. To do this, we applied DHPG (10 μM) for 10 min while recording eIPSCs in WT and *Fmr1* KO L2/3 pyramidal cells at 0.25 Hz for a total of 40 min. We found that mGluR activation evoked a chemically-induced I-LTD in L2/3 pyramidal cells from WT mice (62.94 ± 4.71% of the baseline, $n = 11$, $p = .0005$; Fig. 4A [upper panel] and C) and that AM251 blocked the chemically-induced I-LTD (99.96 ± 8.60% of the baseline, $n = 3$, $p = .61$; Fig. 4A [lower panel] and C), confirming the participation of mGluR in the phenomena. On the other hand, we found that although direct mGluR activation *via* DHPG in *Fmr1* KO L2/3 pyramidal cells induced significant short-term depression (41.81 ± 4.42% of the baseline, $n = 7$, $p = .001$; Fig. 4B and D), it failed to evoke long-term responses (93.60 ± 7.82% of the baseline, n = 7, $p = .49$; Fig. 4B and D). This suggests that the triggering mechanism for heterosynaptic I-LTD might be intact but cannot be sustained long-term in *Fmr1* KOs when chemically induced as opposed to electrical induction. Taken together, these data suggest three important phenomena: 1) that inhibitory drive onto L2/3 pyramidal cells of the somatosensory cortex undergo a mGluR-mediated heterosynaptic I-LTD in WT mice that is similar to previous reports (Chevaleyre and Castillo, 2003), 2) that I-LTD plasticity is abnormal in the L2/3 of the somatosensory cortex of *Fmr1* KOs and 3) that faulty I-LTD responses in *Fmr1* KO mice can either be due to a hyperactivated inhibitory network that cannot further be stimulated or a diminished sensitivity of mGluRs.

### 5.1. The eCB neurotransmission system is not responsible for altered I-LTD in Fmr1 KO mice

Since blocking CB1R activation with AM251 revealed that electrical and chemically induced I-LTD is dependent on intracellular endocannabinoid (eCB) mobilization (Figs. 3 and 4), we next wanted to determine whether eCB mobilization mechanisms are responsible for the faulty I-LTD seen in *Fmr1* KOs (Fig. 5). To do this, we examined depolarization suppression of inhibition (DSI). DSI is a known form of short-term plasticity dependent on trans-synaptic eCB mobilization that is triggered by the depolarization of the postsynaptic neuron resulting in decreased GABA release from the presynaptic inhibitory interneuron (Varma et al., 2001). This mechanism resembles the first steps of the I-LTD phenomena and allows us to test whether eCB mobilization mechanisms are functional. In this experiment, because interneuronal populations that are sensitive to mAchR modulation overlap with CB1R-expressing interneurons, we bath applied carbachol (10 μM) to increase the amplitude of the inhibitory drive that is mediated by eCB-sensitive interneurons in L2/3. This strategy has been used before by other researchers to better study the DSI phenomena (Nagode et al., 2014; Vargish et al., 2017). As a result, when L2/3 pyramidal cells were depolarized from −60 to 0 mV for 1 s, sIPSC amplitudes were depressed from the original amplitude in WT (39.24 ± 7.66%, $n = 5$) and in *Fmr1* KOs (51.87 ± 9.38%, $n = 9$), indicating no significant differences in DSI between *Fmr1* KO *versus* WT mice ($p = .32$; Fig. 5A, D, and E). These responses also have similar latencies and time courses for WT and *Fmr1* KO L2/3 pyramidal cells (Fig. 4D). These results indicate that eCB storage and mobilization are functional in the *Fmr1* KO mouse model suggesting that the abnormalities seen in I-LTD are not due to deficiencies in these eCB system properties. Finally, to determine if disrupted I-LTD may be due to deficits in CB1R function, we tested the effect of Win55 (5 μM), a CB1R agonist, in eIPSCs recorded from L2/3 pyramidal cells of WT and *Fmr1* KO mice. We found that an equal subset of pyramidal cells were depressed in response to Win55 in WT (7/11) and *Fmr1* KO (3/5) with no statistical differences in the magnitude of the CB1R response (42.47 ± 2.21%, $n = 7$, $p = 1.52e\text{-}6$, and 54.83 ± 2.04%, $n = 3$, $p = .011$) (Fig. 5B,C, and F). Thus, we conclude that CB1R sensitivity and the eCB neurotransmission system are not directly responsible in determining the faulty long-term I-LTD seen in *Fmr1* KOs.

## 6. Discussion

The hyperexcitable phenotype observed in FXS is largely attributed to excessive excitatory drive, yet the role of inhibitory contributions is less understood. Moreover, plasticity at inhibitory synapses is under-studied in light of several studies that have documented faulty synaptic plasticity in *Fmr1* KOs. Here, we demonstrate abnormalities in the inhibitory network activity and in mechanisms that dictate inhibitory plasticity and function in L2/3 pyramidal cells in somatosensory cortex of *Fmr1* KO mice. Overall, we observe basal hyperexcitability and an increase in neuronal firing rate suppression during whisker activation *in vivo* and increased basal inhibitory spontaneous currents, a faulty mGluR-mediated activation of inhibitory events, and impaired depressive plasticity at inhibitory synapses *in vitro*. These phenomena result in an overall enhanced cortical inhibitory synaptic function in L2/3 of the primary somatosensory cortex of *Fmr1* KO mice that could

potentially mediate a homeostatic counterbalance to the hyperexcitability of FXS cortical circuits found *in vivo*.

## 7. *Fmr1* KO S1 L2/3 neurons show hyperexcitability and augmented sensory response

Previous behavioral experiments have shown that *Fmr1* KO mice exhibit an exaggerated response to whisker stimulation, a failure to adapt to repetitive stimuli and an impaired learning in a whisker-dependent behavioral task (Arnett et al., 2014; He et al., 2017). At the neuronal level, *in vivo* experiments have shown that neurons of the somatosensory cortex are hyperexcited (Goncalves et al., 2013; Zhang et al., 2014). In agreement with this, we found that neurons in *Fmr1* KOs fired at a higher rate in basal conditions throughout different brain states (anesthetized and awake). Interestingly, a recent study presented results suggesting that spontaneous basal cortical activity is similar in both *Fmr1* KO and WT animals (Antoine et al., 2019). Thus presenting a situation which deviates from our findings and others (Goncalves et al., 2013; Zhang et al., 2014). We believe these differences in anesthetized and awake recording results may rely on experimental design. Specifically, we used different anesthesia drugs (isoflurane *vs* urethane/chlorprothixene) and awake behavioral paradigms (freely moving *vs* head fixed) in our experiments, both possibly having an impact on network excitability and the outcome of these experiments. Moreover, they show that neurons in the L2/3 of the *Fmr1* KO exhibit spatially broader cortical activation to single-whisker stimulation and a decreased whisker-evoked firing rates in response to multiple deflection velocities (Antoine et al., 2019). In agreement with these results, we found that neurons responded differently to stimulus, since more cortical neurons in the *Fmr1* KO mice decreased their FR in response to a single air puff when compared to WT mice. In this case, whisker stimulation is probably robust enough in both scenarios to engage the network overpowering the basal level activity differences. We also found that DHPG infusion on average increased the FR in both WT and *Fmr1* KO L2/3 neurons *in vivo*. However, there was a trend showing a diminished FR increments (Fig. 1F) in response to mGluR activation in *Fmr1* KO mice; although statistical differences were not detected between genotypes. This could suggest either diminished mGluR sensitivity or an activity ceiling effect that overall restrains the network to reach increased firing rate activity. Understanding that the complexity of the data collected from the somatosensory cortical network could hide relevant information at the cellular level in this context, therefore we performed the *in vitro* experiments.

Taken together, our data suggests that interneuron activity might attempt to counteract alterations in somatosensory coding. Additional *in vivo* electrophysiological experiments could elucidate how different types of somatosensory inputs affect neuronal and network activity in L2/3 and how population coding within all cortical layers leads to hypersensitive driven behaviors seen in FXS. Moreover, selective identification and neuronal activity regulation of different neuronal populations, with techniques such as optogenetic, could shed light on the role excitatory and inhibitory neurons play *in vivo*.

### 7.1. Enhanced inhibitory cortical activity impacts mGluR-mediated modulation

Similar to our results found *in vivo*, we found increased basal neuronal activity in *Fmr1* KO mice. In particular, inhibitory spontaneous activity was higher than in WTs. Although others reported that inhibition is decreased in the somatosensory cortex of *Fmr1* KO, our results do not contradict this finding (Antoine et al., 2019). While their finding is in the context of feedforward inhibition from L4 to L2/3, which is driven by a specific cortical circuit, we find that basal sIPSCs are elevated in *Fmr1* KO mice, which is a read out of the overall inhibitory activity in the network within L2/3. We postulate that the observed elevated basal sIPSC activity is most likely caused by an increased excitatory neurotransmission that drives more inhibition into L2/3 pyramidal cells and/or hyperactive interneuron subtypes that are attempting to homeostatically counterbalance cortical hyperexcitability. Moreover, we found a decreased mGluR-driven spontaneous inhibitory postsynaptic input to pyramidal cells in *Fmr1* KO mice. This loss of mGluR responsiveness could be due to a ceiling effect caused by the hyperactive network, although we cannot discard mGluR changes in expression, decreased membrane localization or structural abnormalities.

### 7.2. Inhibitory plasticity is altered in Fmr1 KO mice

At this time, we are the first to demonstrate that, in contrast to excitatory synapses, LTD at inhibitory synapses (I-LTD) is abolished in the *Fmr1* KO mice. Although these two LTD processes (excitatory and inhibitory LTDs) follow different mechanistic and intracellular pathways of activation, they have at least one critical point in common - mGluR activation. To this point, our results reveal a faulty mGluR-mediated I-LTD in L2/3 of the somatosensory cortex of *Fmr1* KOs. This I-LTD is also dependent on eCB release, CB1R activation, and PKA function as is suggested by the lack of the I-LTD in WT mice when mGluRs, CB1Rs and PKA activity were blocked. These are all molecular components of a heterosynaptic I-LTD, suggesting that this phenomenon is similar to the one observed in the hippocampus (Chevaleyre and Castillo, 2003; Chevaleyre et al., 2007).

Furthermore, previous reports suggest the possibility of direct participation of a faulty enzymatic complex to synthetize eCB in FXS and show that dysfunctional eCB molecular machinery is altered in excitatory synapses without affecting inhibitory connectivity (Maccarrone et al., 2010; Jung et al., 2012). However, our results indicate that eCB activity is unaltered in terms of release and storage availability of eCBs, and that CB1R receptor sensitivity is maintained in *Fmr1* KO mice. Therefore, faulty eCB synthesis is not likely to be the main cause of this faulty heterosynaptic I-LTD in FXS (Fig. 5). Although this finding does not discard a role for the synthesis of eCBs, it may further support a secondary role for eCB receptor activation in the faulty heterosynaptic I-LTD of the somatosensory cortex.

Taken together, it seems that mGluR-mediated I-LTD is lacking in cortical pyramidal cells from *Fmr1* KO because of diminished mGluR responsiveness due to a ceiling effect associated with a hyperactive neuronal network rather than molecular components malfunction. This type of association has been shown before where network activity levels modify the threshold for synaptic transmission and plasticity (Felix-Oliveira et al., 2014).

### 7.3. Is faulty inhibitory plasticity in Fmr1 KOs cell-type specific?

Based on the mechanisms of inhibitory plasticity, our results suggest different interneuron subtypes are contributing to the abnormal activity of the somatosensory cortex of *Fmr1* KO mice. However, previous reports indicate that Sst-LTS interneurons are especially sensitive to activation *via* mGluRs (Fanselow et al., 2008; Paluszkiewicz et al., 2011). Based on those findings, we speculate that the diminished inhibitory response to DHPG recorded from L2/3 pyramidal cells in *Fmr1* KO S1 could be due to the loss of mGluR activation responsiveness in the Sst-LTS cells. On the other hand, because the mechanism of heterosynaptic I-LTD requires the eCB molecular machinery to be activated, as documented previously (Chevaleyre et al., 2007), it is highly likely that interneurons participating in this mechanism of plasticity express CB1Rs. The main candidate for this type of response is CB1R-expressing perisomatic-targeting basket cells (BCs) that belong to the 5HT-3R expressing group of interneurons in the cortex (Lee et al., 2010), which are also characterized by the expression of cholecystokinin (CCK), as is documented in hippocampus and cortex (Foldy et al., 2007; De-May and Ali, 2013). The abnormal function of these interneurons, resulting from a faulty mGluR modulation, would have different implications in the activity of the cortical network. Although these two interneuron cell types (Sst-LTS and CCK-BCs) modulate the network in similar fashion by having a role in the fine tuning of the information being processed in the cortex (Lee et al., 2010; Rudy et al., 2011), they have different postsynaptic targets (perisomatic *vs* dendritic) and timing of the response associated to mGluR activation (short *vs* long-term) (Chevaleyre and Castillo, 2003; Marinelli et al., 2008). Thus, we speculate that the faulty modulation on the dendritic targeting Sst-LTS cells would lead to an immediate but transient truncated inhibitory control over the excitatory activity of the somatosensory cortex, and the unregulated I-LTD mediated by CCK-BCs would lead to a loss of the long-term control of the inhibitory drive in the *Fmr1* KO mice. Interestingly, PV-positive interneurons have been shown to decrease their output activity in the *Fmr1* KO cortex (Gibson et al., 2008; Goel et al., 2018; Antoine et al., 2019) suggesting a diminished inhibitory drive in the network opposite to what is presented here; however, our data does not contradict those findings, considering that interneurons have different properties in the network and their contribution to the phenotype is cell-type specific in the somatosensory cortex.

In a like manner, the mAchR response reported here could also be determined by interneuron classes. Interestingly, we found that mAChR-mediated I-LTD is disrupted in *Fmr1* KO mice and that carbachol-enhanced inhibitory drive in our DSI experiment is not. We think that although these are opposites effects on the inhibitory drive in our I-LTD and DSI experiments, this is expected considering the differences in experimental designs. I-LTD is done by electrical stimulation of L4 of somatosensory cortex, leading to eIPSCs mediated by different inhibitory cells where only a fraction can be eCB downregulated, and DSI is measured by sIPSCs where mAchR activation selectively enhances the inhibitory responses of those cells that can be modulated by eCB release, giving a more specific downregulation of the inhibitory activity. Thus, mAchR activation during I-LTD and DSI responses incorporate different cellular components. Lastly, despite the fact that M4 mAchR translation is upregulated in *Fmr1* KO mice and its activation can restore both protein synthesis levels and excitatory LTD in the hippocampus (Thomson et al., 2017), the mAchR

activation in *Fmr1* KO in this study did not restore the I-LTD phenomena seen in WT mice, possibly as a result of our nonspecific treatment.

## 8. Conclusion

The findings of this manuscript suggest that cortical network inhibition is attempting to counterbalance the hyperexcitability observed in the *Fmr1* KO mouse model of FXS. At baseline levels, inhibitory synaptic activity (in the form of sIPSCs) is higher in the somatosensory cortex of *Fmr1* KOs suggesting there is an attempt to balance the heightened levels of excitatory activity observed in this disorder (Wang et al., 2017). Additionally, in the long-term, inhibition is enhanced in the form of a faulty I-LTD, which allows a persistent inhibitory drive into postsynaptic cells in periods of long-lasting high cortical network activity. Indeed, the loss of mGluR activation responsiveness in the *Fmr1* KOs could be explained by the increased basal inhibitory drive in the disorder, seemingly at ceiling levels. This would limit the role of mGluRs on activating the network at both baseline and long-term levels. Additionally, this heightened activity likely comes at the cost of a loss of inhibitory synaptic plasticity and signal to noise cortical detection. The influence of this hyperactive cortical network was recently demonstrated by Domanski and colleagues where they showed that during recurrent activity at behaviorally-relevant frequencies, there is decreased and disorganized spiking of L4 neurons (the major excitatory input to L2/3) (Domanski et al., 2019). This would also suggest that sensory information being relayed to L2/3 is most likely dramatically altered (Domanski et al., 2019). Altogether, these data suggest that heightened inhibition is attempting to maintain E/I balance. However, enhanced excitatory and inhibitory activity in the network could lead to faulty sensory signal detection, codification and interpretation resulting in altered somatosensory perception as seen in FXS.

## Acknowledgements

This work was supported by U.S. National Institutes of Health grants (R01 DC000566 to D.R., R01 NS095311 to M.M.H) and FRAXA and FONDECYT #11150816 to CAC-dR. We thank Felipe Avello for help with graphical art.

## References

Antoine MW, Langberg T, Schnepel P, Feldman DE, 2019. Increased excitation-inhibition ratio stabilizes synapse and circuit excitability in four autism mouse models. Neuron 101 (648–661), e644.

Arnett MT, Herman DH, McGee AW, 2014. Deficits in tactile learning in a mouse model of fragile X syndrome. PLoS ONE 9, e109116. [PubMed: 25296296]

Auerbach BD, Bear MF, 2010. Loss of the fragile X mental retardation protein de-couples metabotropic glutamate receptor dependent priming of long-term potentiation from protein synthesis. J. Neurophysiol 104, 1047–1051. [PubMed: 20554840]

Bagni C, Greenough WT, 2005. From mRNP trafficking to spine dysmorphogenesis: the roots of fragile X syndrome. Nat. Rev. Neurosci 6, 376–387. [PubMed: 15861180]

Bear MF, Huber KM, Warren ST, 2004. The mGluR theory of fragile X mental retardation. Trends Neurosci. 27, 370–377. [PubMed: 15219735]

Bianchi R, Chuang SC, Zhao W, Young SR, Wong RK, 2009. Cellular plasticity for group I mGluR-mediated epileptogenesis. J. Neurosci 29, 3497–3507. [PubMed: 19295155]

Brown V, Jin P, Ceman S, Darnell JC, O'Donnell WT, Tenenbaum SA, Jin X, Feng Y, Wilkinson KD, Keene JD, Darnell RB, Warren ST, 2001. Microarray identification of FMRP-associated brain mRNAs and altered mRNA translational profiles in fragile X syndrome. Cell 107, 477–487. [PubMed: 11719188]

Castillo PE, Chiu CQ, Carroll RC, 2011. Long-term plasticity at inhibitory synapses. Curr. Opin. Neurobiol 21, 328–338. [PubMed: 21334194]

Chevaleyre V, Castillo PE, 2003. Heterosynaptic LTD of hippocampal GABAergic synapses: a novel role of endocannabinoids in regulating excitability. Neuron 38, 461–472. [PubMed: 12741992]

Chevaleyre V, Heifets BD, Kaeser PS, Sudhof TC, Castillo PE, 2007. Endocannabinoid-mediated long-term plasticity requires cAMP/PKA signaling and RIM1alpha. Neuron 54, 801–812. [PubMed: 17553427]

Chevere-Torres I, Kaphzan H, Bhattacharya A, Kang A, Maki JM, Gambello MJ, Arbiser JL, Santini E, Klann E, 2012. Metabotropic glutamate receptor-dependent long-term depression is impaired due to elevated ERK signaling in the DeltaRG mouse model of tuberous sclerosis complex. Neurobiol. Dis 45, 1101–1110. [PubMed: 22198573]

Connor SA, Hoeffer CA, Klann E, Nguyen PV, 2011. Fragile X mental retardation protein regulates heterosynaptic plasticity in the hippocampus. Learn. Mem 18, 207–220. [PubMed: 21430043]

Contractor A, Klyachko VA, Portera-Cailliau C, 2015. Altered neuronal and circuit excitability in fragile X syndrome. Neuron 87, 699–715. [PubMed: 26291156]

Curran-Everett D, 2000. Multiple comparisons: philosophies and illustrations. Am. J. Phys. Regul. Integr. Comp. Phys 279, R1–R8.

De-May CL, Ali AB, 2013. Cell type-specific regulation of inhibition via cannabinoid type 1 receptors in rat neocortex. J. Neurophysiol 109, 216–224. [PubMed: 23054605]

D'Hulst C, De Geest N, Reeve SP, Van Dam D, De Deyn PP, Hassan BA, Kooy RF, 2006. Decreased expression of the GABAA receptor in fragile X syndrome. Brain Res. 1121, 238–245. [PubMed: 17046729]

Doischer D, Hosp JA, Yanagawa Y, Obata K, Jonas P, Vida I, Bartos M, 2008. Postnatal differentiation of basket cells from slow to fast signaling devices. J. Neurosci 28, 12956–12968. [PubMed: 19036989]

Domanski APF, Booker SA, Wyllie DJA, Isaac JTR, Kind PC, 2019. Cellular and synaptic phenotypes lead to disrupted information processing in Fmr1-KO mouse layer 4 barrel cortex. Nat. Commun 10, 4814. [PubMed: 31645553]

Doucette W, Gire DH, Whitesell J, Carmean V, Lucero MT, Restrepo D, 2011. Associative cortex features in the first olfactory brain relay station. Neuron 69, 1176–1187. [PubMed: 21435561]

Ebert DH, Greenberg ME, 2013. Activity-dependent neuronal signalling and autism spectrum disorder. Nature 493, 327–337. [PubMed: 23325215]

El Idrissi A, Ding XH, Scalia J, Trenkner E, Brown WT, Dobkin C, 2005. Decreased GABA(a) receptor expression in the seizure-prone fragile X mouse. Neurosci. Lett 377, 141–146. [PubMed: 15755515]

Fanselow EE, Richardson KA, Connors BW, 2008. Selective, state-dependent activation of somatostatin-expressing inhibitory interneurons in mouse neocortex. J. Neurophysiol 100, 2640–2652. [PubMed: 18799598]

Felix-Oliveira A, Dias RB, Colino-Oliveira M, Rombo DM, Sebastiao AM, 2014. Homeostatic plasticity induced by brief activity deprivation enhances long-term potentiation in the mature rat hippocampus. J. Neurophysiol 112, 3012–3022. [PubMed: 25210161]

Foldy C, Lee SY, Szabadics J, Neu A, Soltesz I, 2007. Cell type-specific gating of perisomatic inhibition by cholecystokinin. Nat. Neurosci 10, 1128–1130. [PubMed: 17676058]

Gibson JR, Bartley AF, Hays SA, Huber KM, 2008. Imbalance of neocortical excitation and inhibition and altered UP states reflect network hyperexcitability in the mouse model of fragile X syndrome. J. Neurophysiol 100, 2615–2626. [PubMed: 18784272]

Gire DH, Whitesell JD, Doucette W, Restrepo D, 2013. Information for decision-making and stimulus identification is multiplexed in sensory cortex. Nat. Neurosci 16, 991–993. [PubMed: 23792942]

Goel A, Cantu DA, Guilfoyle J, Chaudhari GR, Newadkar A, Todisco B, de Alba D, Kourdougli N, Schmitt LM, Pedapati E, Erickson CA, Portera-Cailliau C, 2018. Impaired perceptual learning in

a mouse model of Fragile X syndrome is mediated by parvalbumin neuron dysfunction and is reversible. Nat. Neurosci 21, 1404–1411. [PubMed: 30250263]

Goldberg EM, Jeong HY, Kruglikov I, Tremblay R, Lazarenko RM, Rudy B, 2011. Rapid developmental maturation of neocortical FS cell intrinsic excitability. Cereb. Cortex 21, 666–682. [PubMed: 20705896]

Goncalves JT, Anstey JE, Golshani P, Portera-Cailliau C, 2013. Circuit level defects in the developing neocortex of fragile X mice. Nat. Neurosci 16, 903–909. [PubMed: 23727819]

Hagerman PJ, Stafstrom CE, 2009. Origins of epilepsy in fragile X syndrome. Epilepsy Curr. 9, 108–112. [PubMed: 19693328]

He CX, Cantu DA, Mantri SS, Zeiger WA, Goel A, Portera-Cailliau C, 2017. Tactile defensiveness and impaired adaptation of neuronal activity in the Fmr1 Knock-out mouse model of autism. J. Neurosci 37, 6475–6487. [PubMed: 28607173]

Huber KM, Gallagher SM, Warren ST, Bear MF, 2002. Altered synaptic plasticity in a mouse model of fragile X mental retardation. Proc. Natl. Acad. Sci. U. S. A 99, 7746–7750. [PubMed: 12032354]

Huntsman MM, Huguenard JR, 2000. Nucleus-specific differences in GABA(A)-receptor-mediated inhibition are enhanced during thalamic development. J. Neurophysiol 83, 350–358. [PubMed: 10634878]

Jung KM, Sepers M, Henstridge CM, Lassalle O, Neuhofer D, Martin H, Ginger M, Frick A, DiPatrizio NV, Mackie K, Katona I, Piomelli D, Manzoni OJ, 2012. Uncoupling of the endocannabinoid signalling complex in a mouse model of fragile X syndrome. Nat. Commun 3, 1080. [PubMed: 23011134]

Kuhn B, Denk W, Bruno RM, 2008. In vivo two-photon voltage-sensitive dye imaging reveals top-down control of cortical layers 1 and 2 during wakefulness. Proc. Natl. Acad. Sci. U. S. A 105, 7588–7593. [PubMed: 18508976]

Lee S, Hjerling-Leffler J, Zagha E, Fishell G, Rudy B, 2010. The largest group of superficial neocortical GABAergic interneurons expresses ionotropic serotonin receptors. J. Neurosci 30, 16796–16808. [PubMed: 21159951]

Li A, Gire DH, Restrepo D, 2015a. Y spike-field coherence in a population of olfactory bulb neurons differentiates between odors irrespective of associated outcome. J. Neurosci 10.1523/JNEUROSCI.4003-14.201 in press.

Li A, Gire DH, Bozza T, Restrepo D, 2014. Precise detection of direct glomerular input duration by the olfactory bulb. J. Neurosci 34, 16058–16064. [PubMed: 25429146]

Li A, Gire DH, Restrepo D, 2015b. Upsilon spike-field coherence in a population of olfactory bulb neurons differentiates between odors irrespective of associated outcome. J. Neurosci 35, 5808–5822. [PubMed: 25855190]

Maccarrone M, Rossi S, Bari M, De Chiara V, Rapino C, Bernardi G, Bagni C, Centonze D, 2010. Abnormal mGlu 5 receptor/endocannabinoid coupling in mice lacking FMRP and BC1 RNA. Neuropsychopharmacology 35, 1500–1509. [PubMed: 20393458]

Maffei A, 2017. Fifty shades of inhibition. Curr. Opin. Neurobiol 43, 43–47. [PubMed: 28012992]

Marinelli S, Pacioni S, Bisogno T, Di Marzo V, Prince DA, Huguenard JR, Bacci A, 2008. The endocannabinoid 2-arachidonoylglycerol is responsible for the slow self-inhibition in neocortical interneurons. J. Neurosci 28, 13532–13541. [PubMed: 19074027]

Martin BS, Corbin JG, Huntsman MM, 2014. Deficient tonic GABAergic conductance and synaptic balance in the fragile X syndrome amygdala. J. Neurophysiol 112, 890–902. [PubMed: 24848467]

Miller LJ, McIntosh DN, McGrath J, Shyu V, Lampe M, Taylor AK, Tassone F, Neitzel K, Stackhouse T, Hagerman RJ, 1999. Electrodermal responses to sensory stimuli in individuals with fragile X syndrome: a preliminary report. Am. J. Med. Genet 83, 268–279. [PubMed: 10208160]

Nagode DA, Tang AH, Yang K, Alger BE, 2014. Optogenetic identification of an intrinsic cholinergically driven inhibitory oscillator sensitive to cannabinoids and opioids in hippocampal CA1. J. Physiol 592, 103–123. [PubMed: 24190932]

Nosyreva ED, Huber KM, 2006. Metabotropic receptor-dependent long-term depression persists in the absence of protein synthesis in the mouse model of fragile X syndrome. J. Neurophysiol 95, 3291–3295. [PubMed: 16452252]

Olmos-Serrano JL, Paluszkiewicz SM, Martin BS, Kaufmann WE, Corbin JG, Huntsman MM, 2010. Defective GABAergic neurotransmission and pharmacological rescue of neuronal hyperexcitability in the amygdala in a mouse model of fragile X syndrome. J. Neurosci 30, 9929–9938. [PubMed: 20660275]

Paluszkiewicz SM, Olmos-Serrano JL, Corbin JG, Huntsman MM, 2011. Impaired inhibitory control of cortical synchronization in fragile X syndrome. J. Neurophysiol 106, 2264–2272. [PubMed: 21795626]

Quiroga RQ, Nadasdy Z, Ben-Shaul Y, 2004. Unsupervised spike detection and sorting with wavelets and superparamagnetic clustering. Neural Comput. 16, 1661–1687. [PubMed: 15228749]

Rudy B, Fishell G, Lee S, Hjerling-Leffler J, 2011. Three groups of interneurons account for nearly 100% of neocortical GABAergic neurons. Develop. Neurobiol 71, 45–61.

Song C, Piscopo DM, Niell CM, Knopfel T, 2018. Cortical signatures of wakeful somatosensory processing. Sci. Rep 8, 11977. [PubMed: 30097603]

Thomson SR, Seo SS, Barnes SA, Louros SR, Muscas M, Dando O, Kirby C, Wyllie DJA, Hardingham GE, Kind PC, Osterweil EK, 2017. Cell-type-specific translation profiling reveals a novel strategy for treating fragile X syndrome. Neuron 95 (550–563), e555.

Vargish GA, Pelkey KA, Yuan X, Chittajallu R, Collins D, Fang C, McBain CJ, 2017. Persistent inhibitory circuit defects and disrupted social behaviour following in utero exogenous cannabinoid exposure. Mol. Psychiatry 22, 56–67. [PubMed: 26976041]

Varma N, Carlson GC, Ledent C, Alger BE, 2001. Metabotropic glutamate receptors drive the endocannabinoid system in hippocampus. J. Neurosci 21, RC188. [PubMed: 11734603]

Wang J, Ethridge LE, Mosconi MW, White SP, Binder DK, Pedapati EV, Erickson CA, Byerly MJ, Sweeney JA, 2017. A resting EEG study of neocortical hyperexcitability and altered functional connectivity in fragile X syndrome. J. Neurodev. Disord 9, 11. [PubMed: 28316753]

Yau SY, Bostrom CA, Chiu J, Fontaine CJ, Sawchuk S, Meconi A, Wortman RC, Truesdell E, Truesdell A, Chiu C, Hryciw BN, Eadie BD, Ghilan M, Christie BR, 2016. Impaired bidirectional NMDA receptor dependent synaptic plasticity in the dentate gyrus of adult female Fmr1 heterozygous knockout mice. Neurobiol. Dis 96, 261–270. [PubMed: 27659109]

Younts TJ, Castillo PE, 2014. Endogenous cannabinoid signaling at inhibitory interneurons. Curr. Opin. Neurobiol 26, 42–50. [PubMed: 24650503]

Younts TJ, Chevaleyre V, Castillo PE, 2013. CA1 pyramidal cell theta-burst firing triggers endocannabinoid-mediated long-term depression at both somatic and dendritic inhibitory synapses. J. Neurosci 33, 13743–13757. [PubMed: 23966696]

Zhang J, Hou L, Klann E, Nelson DL, 2009. Altered hippocampal synaptic plasticity in the FMR1 gene family knockout mouse models. J. Neurophysiol 101, 2572–2580. [PubMed: 19244359]

Zhang Y, Bonnan A, Bony G, Ferezou I, Pietropaolo S, Ginger M, Sans N, Rossier J, Oostra B, LeMasson G, Frick A, 2014. Dendritic channelopathies contribute to neocortical and sensory hyperexcitability in Fmr1(−/y) mice. Nat. Neurosci 17, 1701–1709. [PubMed: 25383903]

Zoghbi HY, 2003. Postnatal neurodevelopmental disorders: meeting at the synapse? Science 302, 826–830. [PubMed: 14593168]

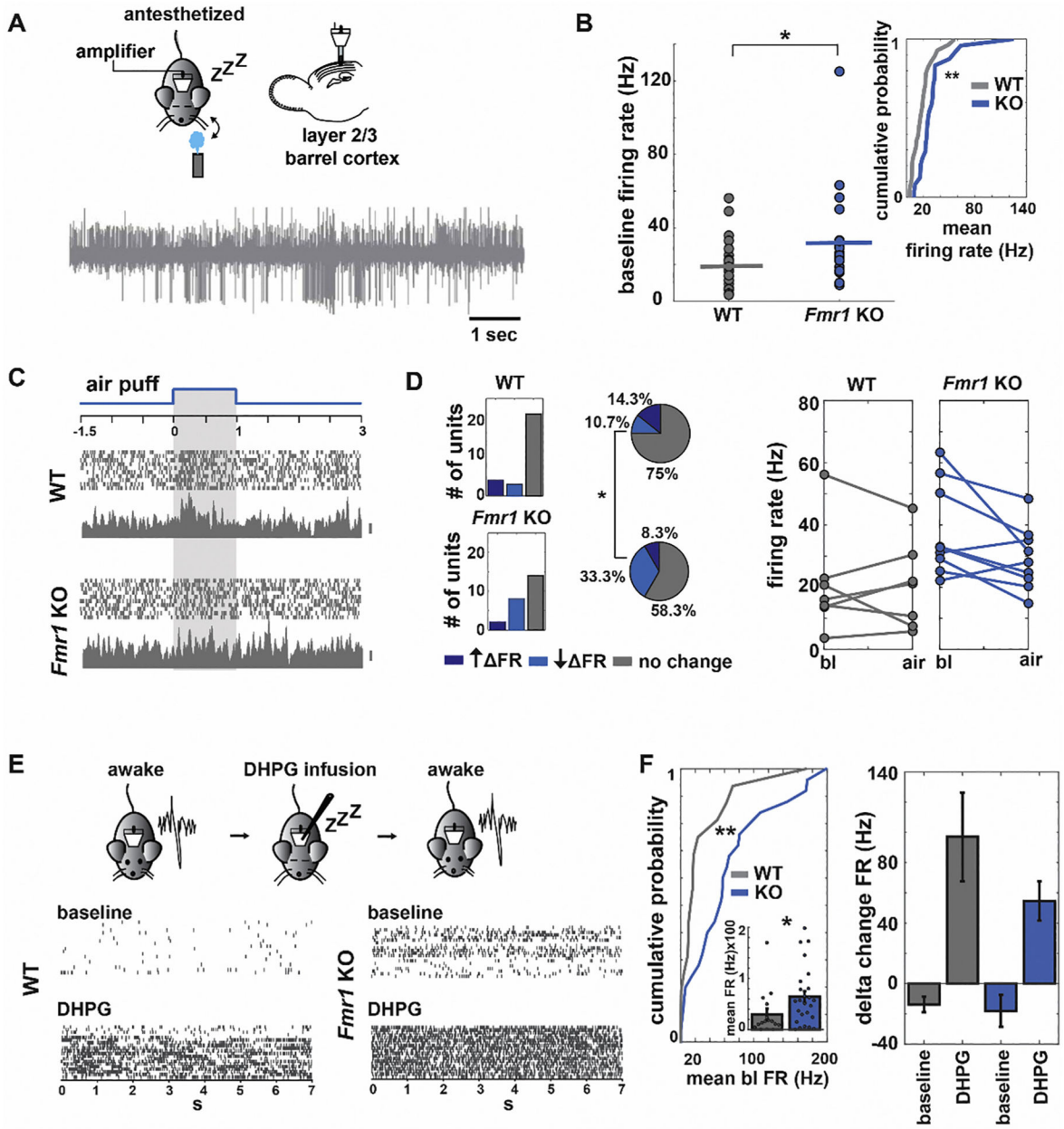


**Fig. 1.**

S1 L2/3 neurons exhibit basal hyperexcitability and an increase in neuronal firing rate suppression during whisker activation in *Fmr1* KOs.

(A) Upper panels: Diagram of the experimental set-up of *in vivo* electrophysiological recording in anesthetized mice. Mice implanted in L2/3 with a movable device with 4 tetrodes were anesthetized and contralateral whiskers were stimulated with an air puff (~3 L/min). Bottom panel: representative electrophysiological recording of one electrode. (B) Comparison of the basal firing rate of all the neurons recorded in the WT (grey) and *Fmr1* KO (blue; $n = 29$ units from 3 WT and $n = 24$ units from 3 *Fmr1* KO; mean ± S.E.M; $^{**}p = .02$). Inset: cumulative probability function of the data (K–S test $p < .005$) (C) Left: representative excitatory response (10 trials, spikes and peristimulus time histogram (PSTH)

shown, bar 10 spikes) of two units (top panel WT, bottom panel, *Fmr1* KO) in response to the stimulus. The air puff was delivered for 1 s. Right: population graph depicting the number and percentage of units that exhibited a statistically significant increase, decrease or no change in FR after stimulus delivery. (D) Left, bar graph showing units separated by their statistical change in firing rate (FR) before and after stimulus presentation in the WT and KO response to the air puff (determined by a *t*-test corrected for multiple comparison, $*p = .04$) and population graph depicting the number and percentage of units that exhibited a statistically significant increase, decrease or no change in FR after stimulus delivery. Right, summary of the neuronal response to air puff of the units that exhibited a statistical change in FR after the air puff. (E) Top, diagram of experimental design of DHPG infusion. Twenty trials of baseline activity were recorded in the awake and freely moving mouse. The mouse was then anesthetized and DHPG (100 μM) was infused directly into L2/3. 30 min after infusion, twenty trials of extracellular activity were recorded. Bottom, representative raster plots of a unit during baseline condition and after DHPG infusion in the WT and *Fmr1* KO. (F) Left, cumulative probability analysis of the mean baseline FR of awake and freely moving WT and *Fmr1* KO mice ($n = 16$ units and $n = 25$ units from 3 WT and 3 *Fmr1* KO, respectively; mean ± S.E.M; $**p = .008$). Left inset, bar graph describing the mean basal firing rate with scatter plot overlaid on top (t-test, $P = .046$). Right, bar graph depicting the delta FR of all the units recorded in basal conditions and after DHPG infusion.

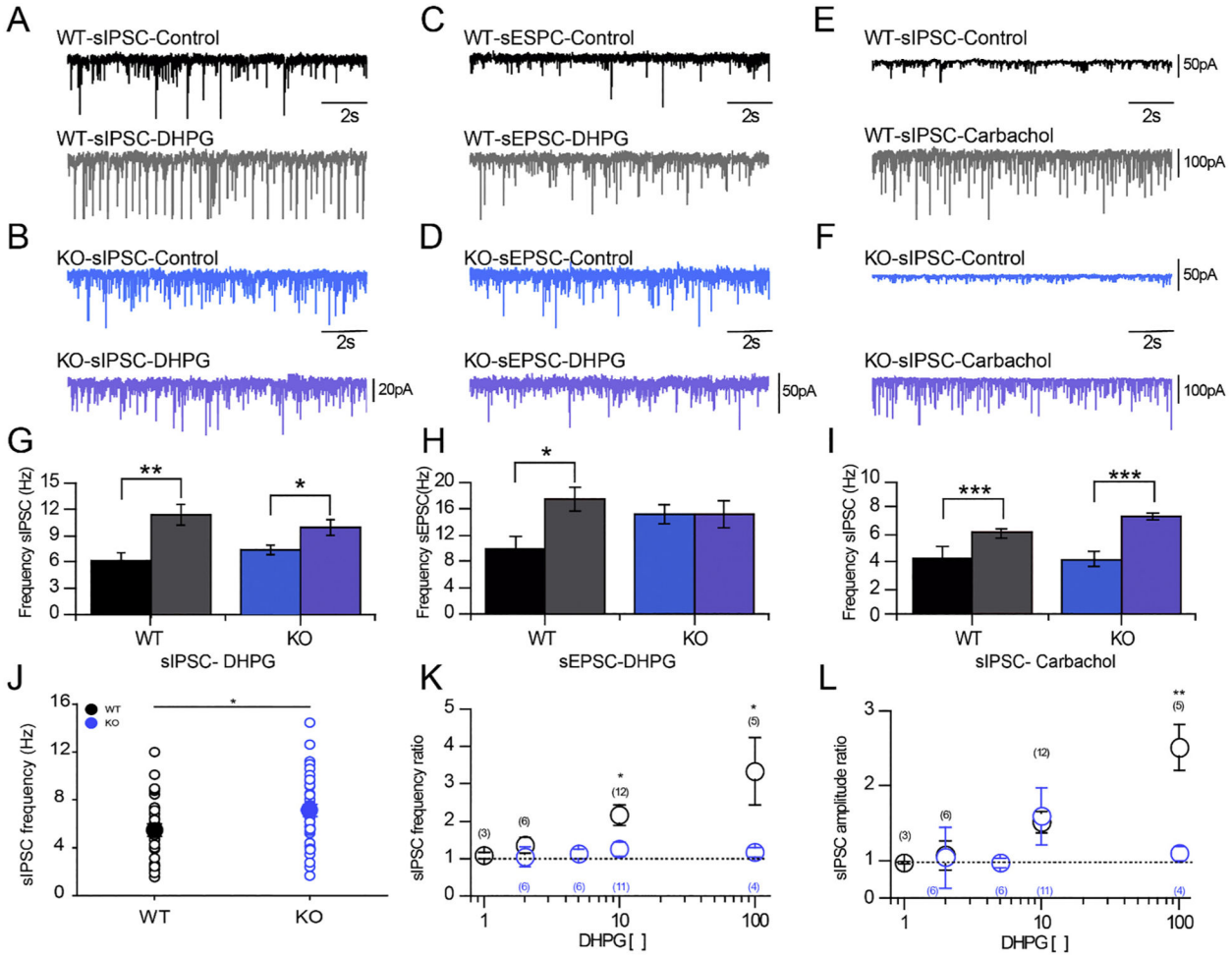


**Fig. 2.**

*In vitro* recordings show augmented basal inhibition and a diminished inhibitory drive mediated by mGluR activation in *Fmr1* KO L2/3 of the somatosensory cortex. (A-D) Representative voltage clamp traces of sIPSC and sEPSC activity before and after application of DHPG (10 μM) from WT and *Fmr1* KO mice, respectively. (*E*-F) Representative voltage clamp traces for sIPSC frequency before and after application of carbachol (10 μM) from WT and *Fmr1* KO mice. (G) Bar population plot of sIPSC frequency from A and B. (H) Bar population plot of sEPSC frequency from C and D (I) Bar population plot of sIPSC frequency from E and F. (J) Single (open) and average (filled) baseline sIPSC frequency from WT and *Fmr1* KO mice. (K-L) Logarithmic population plot of sIPSC frequency ratio and sIPSC amplitude ratio, respectively, before and after application of different concentrations of DHPG from WT (black circles) and *Fmr1* KO (blue circles). All recordings are from L2/3 pyramidal neurons.

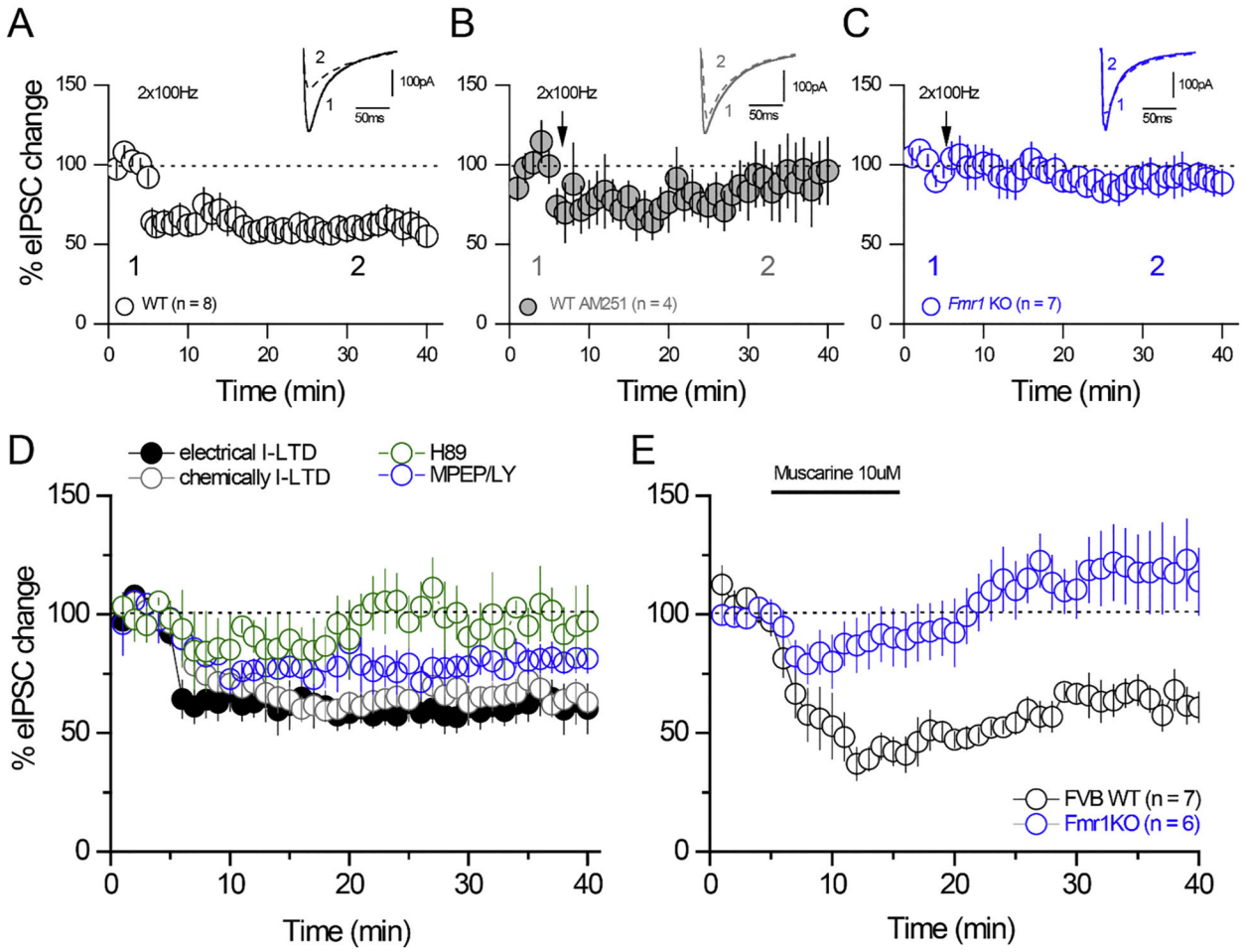


**Fig. 3.**

Heterosynaptic I-LTD is disrupted in L2/3 of *Fmr1* KO mice.

(A) Percentage of eIPSC activity change over time from L2/3 pyramidal cells of WT mice before and after an electrical HFS stimulation and (B) in the presence of AM251 (an eCB receptor inverse agonist). (C) Percentage of eIPSC activity change over time from L2/3 pyramidal cells of *Fmr1* KO mice before and after an electrical HFS stimulation. Inset shows representative eIPSC waveform before (1) and after (2) HFS protocol. (D) Percentage of eIPSC activity change over time from L2/3 pyramidal cells of WT mice before and after an electrical HFS stimulation (black filled circles), chemically-induced protocol (grey open circles), in the presence of a mGluR antagonist cocktail of MPEP/LY367385 (blue open circles) or in the presence of H89 (a PKA inhibitor) (green open circles). (E) Percentage of eIPSC activity change over time from L2/3 pyramidal cells of WT (black circles) and *Fmr1* KO (blue circles) mice before and after 10 min application of muscarine (10 μM).

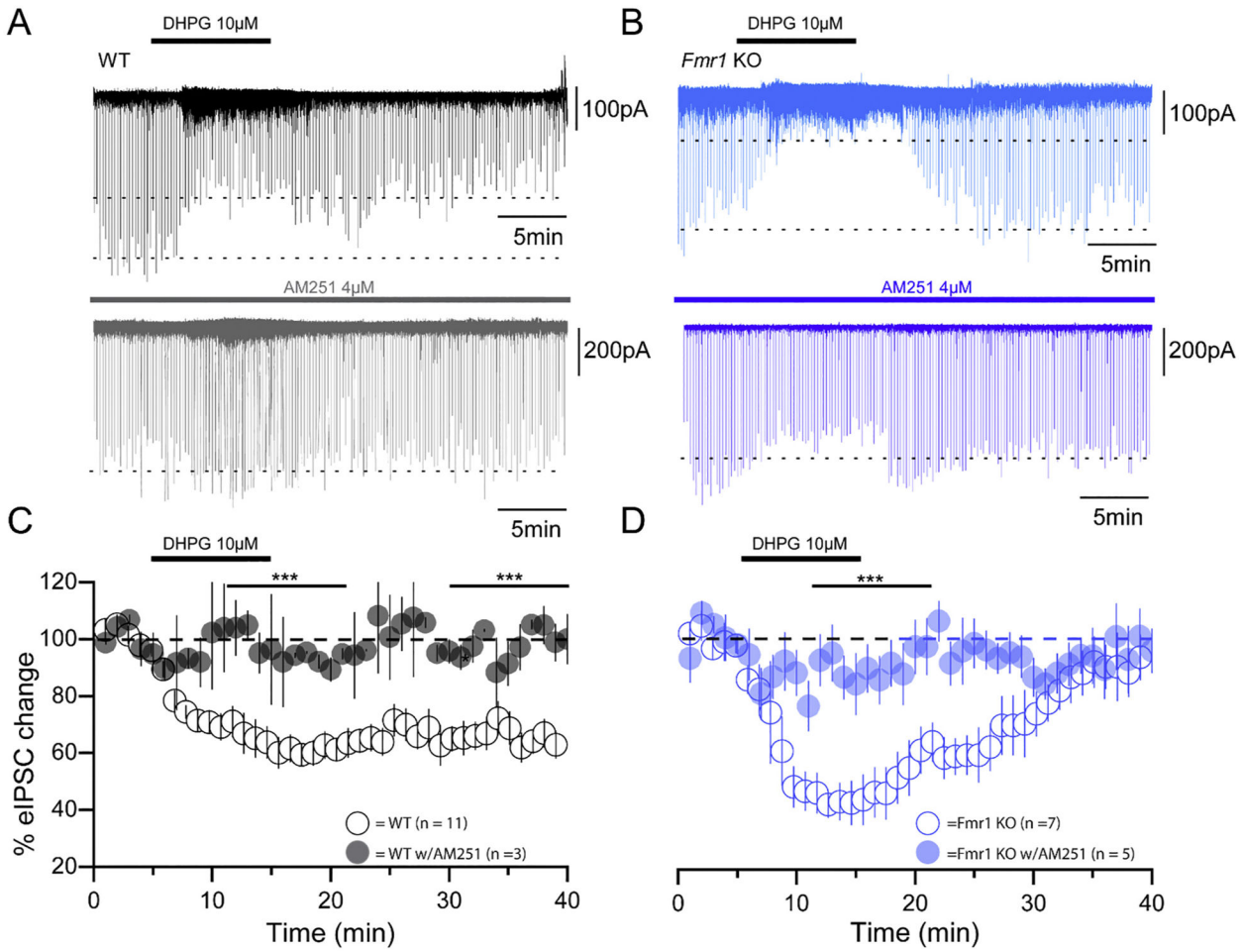


**Fig. 4.**

Chemically induced mGluR activation fails to replicate the heterosynaptic I-LTD in *Fmr1* KO mice.

(A) Representative traces of DHPG-induced I-LTD in pyramidal cells of WT L2/3 in the absence (upper trace) and presence (lower trace) of AM251 (4 μM). (B) Representative traces of DHPG-induced I-LTD in L2/3 pyramidal cells of *Fmr1* KO in the absence (upper trace) and presence of AM251 (lower trace). (C) Percentage of change in eIPSC activity over time from L2/3 pyramidal cell population of WT mice in the absence (open black circles) and presence of AM251 (filled black circles) before and after 10 min application of DHPG (10 μM). (D) Percentage of change in eIPSC activity over time from L2/3 pyramidal cell population of *Fmr1* KO mice in the absence (open blue circles) and presence (filled blue circles) of AM251 before and after 10 min application of DHPG.

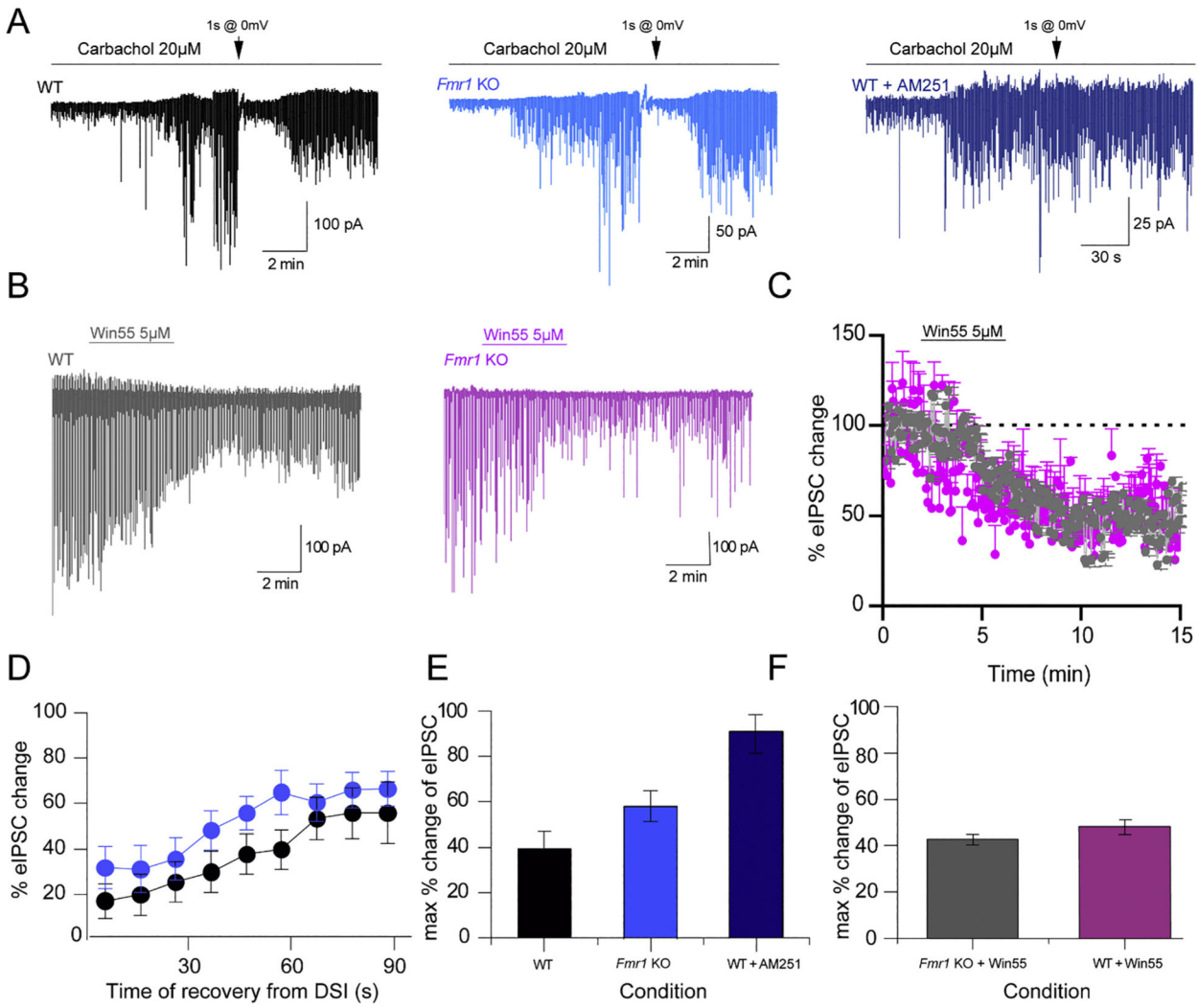


**Fig. 5.**

eCB machinery is intact in *Fmr1* KO mice.

(A) Representative carbachol induced sIPSCs before, and after a DSI protocol of 1 s of depolarization to 0 mV from WT (black traces), *Fmr1* KO (blue traces) and WT in the presence of AM251 (indigo trace) L2/3 pyramidal cell recordings. (B) Representative traces of eIPSCs before and after application of Win55 (5 μM), a CB1R agonist, from WT (black traces) and *Fmr1* KO (violet traces) L2/3 pyramidal cells. (C) Data population of percentage of change in eIPSC activity from WT (grey circles) and *Fmr1* KO (violet circles) L2/3 pyramidal cells in the presence of Win55 (5 μM) from baseline. (D) Data population of percentage of change in eIPSC activity over time 90 s after the DSI induction protocol for WT (black circles) and *Fmr1* KO (blue circles) L2/3 pyramidal cells from baseline. (E) Data population bar plots of maximum percentage of change in eIPSC activity after induction of DSI protocol. (F) Data population bar plots of maximum percentage of change in eIPSC activity after application of Win55 (5 μM).